

The X-ray light curve of Eta Carinae

Julian M. Pittard,^{1★} Ian R. Stevens,^{1★} Michael F. Corcoran^{2★} and Kazunori Ishibashi^{3★}

¹*School of Physics and Astronomy, University of Birmingham, Edgbaston, Birmingham B15 2TT*

²*Universities Space Research Association/Laboratory for High Energy Astrophysics, GSFC, Greenbelt, MD 20771, USA*

³*Astronomy Department, University of Minnesota, 116 Church St. SE, Minneapolis, MN 55455, USA*

Accepted 1998 June 23. Received 1998 June 18; in original form 1998 March 23

ABSTRACT

Following the proposal by Damineli that the central object of Eta Carinae may be an early-type binary, we perform numerical simulations of the X-ray emission from colliding stellar winds. A synthetic light curve has been generated which qualitatively agrees with the recent X-ray variability, and provides further support for the binary model. In particular, the model predicts a rise in the observed X-ray emission towards periastron, followed by a sharp drop and subsequent recovery. This is indeed what is seen in the *RXTE* light curve, although some problems concerning the X-ray spectrum at periastron still need to be explained. The simulations suggest that the width of the periastron dip will provide strong constraints on the binary and stellar wind properties of the components of Eta Car.

Key words: hydrodynamics – binaries: general – stars: early-type – stars: individual: Eta Car – X-rays: stars.

1 INTRODUCTION

Eta Carinae is one of the most mysterious and luminous ($\sim 5 \times 10^6 L_{\odot}$) objects in our Galaxy (Cox et al. 1995). It is best known for a dramatic outburst in 1843 which expelled $\sim 1.0 M_{\odot}$ of material to form the bipolar nebula known as the Homunculus. The nature of the outburst (and the central object) remains controversial. The widely accepted view is that the central object is a luminous blue variable (LBV; Davidson 1989), a massive, evolved star near the Eddington limit, subject to violent instabilities and periods of large mass loss. van Genderen, de Groot & Thé (1994) note that Eta Car shares certain characteristics with the LBV S Dor, where states of quiescence, in which the star is fainter and hotter, alternate with eruptive phases, in which it is cooler and brighter, over time-scales of years to tens of years (Humphreys & Davidson 1994). These phases have been observed in Eta Car, and Damineli (1996) reports a 5.52-yr period which fits all the observed shell episodes in the last 150 yr.

This discovery suggested that Eta Car was a binary, and was substantially reinforced when Damineli, Conti & Lopes (1997) discovered that the 5.52-yr cycle also existed in radial velocity measurements in the Pa γ emission line. The velocity solution indicated a highly eccentric orbit leading to the postulation that Eta Car should show strong wind–wind interaction effects. The orbital parameters have subsequently been improved by Davidson (1997).

Colliding stellar winds are a common feature in early-type binaries. Temperatures in excess of 10^7 K occur in the shock-

heated region generated by the wind collision, which is a strong thermal X-ray source (Stevens, Blondin & Pollock 1992). Eta Car has been extensively observed with *ROSAT*, *ASCA*, and *RXTE* over the most recent 5.52-yr cycle. The observed X-ray emission can be fitted by a two-temperature Raymond–Smith spectral model (Corcoran et al. 1995; Corcoran et al. 1998a). The cool component has $kT \sim 0.4$ keV and $N_{\text{H}} \sim 3.0 \times 10^{21}$ cm $^{-2}$. For the hot component $kT \sim 5.0$ keV and $N_{\text{H}} \sim 4.0 \times 10^{22}$ cm $^{-2}$. The cool emission primarily arises from an extended region surrounding the Homunculus. The hot component is similar to that seen in other colliding-wind systems (eg. HD 193793, Williams et al. 1990; γ^2 Velorum, Willis, Schild & Stevens 1995), although slightly hotter and more absorbed.

In this Letter we propose that the bulk of the observed hard X-ray emission from Eta Car is the result of colliding stellar winds. Since 1996 April, Eta Car has been repeatedly observed with the *RXTE* satellite, generating a well-sampled light curve which allows a comparison with simulated X-ray emission from a colliding-wind hydrodynamic model.

2 THE HYDRODYNAMICAL MODEL

The simulations presented in this Letter use a Lagrangian-remap version of the piecewise parabolic method (PPM; Colella & Woodward 1984). Several improvements to the code, as applied to colliding stellar winds, have been made, the most important of which is the self-consistent inclusion of the radiative acceleration of the winds. Although Eta Car is a wide binary, the wind interaction region extends down into the wind acceleration zones, so that an assumption of terminal velocity winds would be invalid. This may at first appear somewhat surprising, considering the substantial

★E-mail: jmp@star.sr.bham.ac.uk (JMP); irs@star.sr.bham.ac.uk (IRS); corcoran@barneгат.gsfc.nasa.gov (MFC); bish@astro.spa.umn.edu (KI)

separation of the stars (even at periastron), but it is caused by the slow acceleration of the winds and the large radii of the stars. The winds are accelerated assuming a Castor, Abbott & Klein (1975, hereafter CAK) theory with the addition of a finite-disc correction factor. Further details of this implementation can be found in Pittard (1998). The simulations presented in this Letter were performed on a cylindrical 2D grid with constant cell size ($\delta r = \delta z = 7.66 \times 10^{11}$ cm), of dimensions 600×100 zones. Given the long orbital period, the assumption of axisymmetry is probably reasonable.

For the Eta Car simulation we assume an LBV primary and a massive O star as the secondary, with the orbital parameters mostly from Davidson (1997). The adopted stellar and orbital parameters are listed in Tables 1 and 2. The orbital inclination is believed to be $\sim 55\text{--}60^\circ$, as deduced from the appearance of the large-scale bipolar nebula, and we adopt $i = 60^\circ$. A schematic of the orbit is shown in Fig. 1. The direction of Earth is marked, as well as the position of the secondary star relative to the primary at certain orbital phases. Note that at periastron, the line of sight into the system is through the massive LBV wind. The mass function ($12.5 \pm 4.0 M_\odot$) allows a wide range of masses for both components (Davidson 1997). Stellar temperatures are also uncertain, and have been chosen from the proposed ranges of Damiani et al (1997). We also assumed that the primary (LBV) was ~ 3 times more luminous than the secondary. With the adopted values of the stellar radii, the system luminosity is $3.4 \times 10^6 L_\odot$, slightly lower than generally accepted. Previous estimates are $4.0 \times 10^6 L_\odot$ (Damiani et al. 1997) and $5.0 \times 10^6 L_\odot$ (Cox et al. 1995; Davidson & Humphreys 1997). With the assumed luminosity, the primary has an Eddington ratio of 0.92.

Table 1. Stellar parameters.

Parameter	Primary (LBV)	Secondary (O star)
Mass (M_\odot)	70.0	70.0
Radius (R_\odot)	130.0	44.0
Effective temp. (10^3 K)	20.0	27.5
Mass-loss rate ($10^{-5} M_\odot$)	9.7	1.0
Terminal velocity (10^3)	0.93	1.63
Line force parameter, α	0.70	0.54
Line force parameter, k	0.13	0.32

The mass-loss rates are also uncertain. Past estimates have ranged from 3.0×10^{-4} (radio observations, White et al. 1994) to 2.4×10^{-3} (mm observations, Cox et al. 1995), but these were based on a single-star hypothesis. However, our chosen values serve as a starting point, and the results from the simulations performed with these values provide some indications for their future refinement (see Section 3). This also applies to the values chosen for the wind terminal velocities, which are likewise uncertain. Although CAK theory has not yet been extended to LBV stars, the CAK parameters (α and k) were chosen to produce the given mass-loss rates and terminal velocities, and represent the gross wind characteristics adequately.

The X-ray emissivity is computed from a Raymond–Smith plasma code (Raymond & Smith 1977), assuming optically thin thermal emission and ionization equilibrium. The absorption from each cell is calculated by integrating the density along the line of sight to the observer. Solar abundances have been assumed throughout, although we note that a substantial nitrogen overabundance is seen in the surrounding nebulosity (Davidson, Walborn & Gull 1982; Corcoran et al. 1998a). Further details of our implementation of the X-ray calculations can be found in Pittard & Stevens (1997).

The precise values of the mass-loss rates and terminal velocities affect the overall X-ray luminosity of the system, but the qualitative nature of the resulting light curve is relatively insensitive to these parameters.

3 SIMULATION RESULTS

Fig. 2 shows two frames in a time-sequence of the density structure in the numerical model. The stars are represented by white circles.

Table 2. Orbital parameters.

Orbital period, P (d)	2014
Eccentricity, e	0.802
Periastron distance, P_P (au)	3.29
Apastron distance, P_A (au)	28.9
Inclination, i (deg)	60.0
Periastron longitude, ω (deg)	286.0
Distance, D (kpc)	2.6
Interstellar column, N_H (10^{21} cm^{-2})	2.0

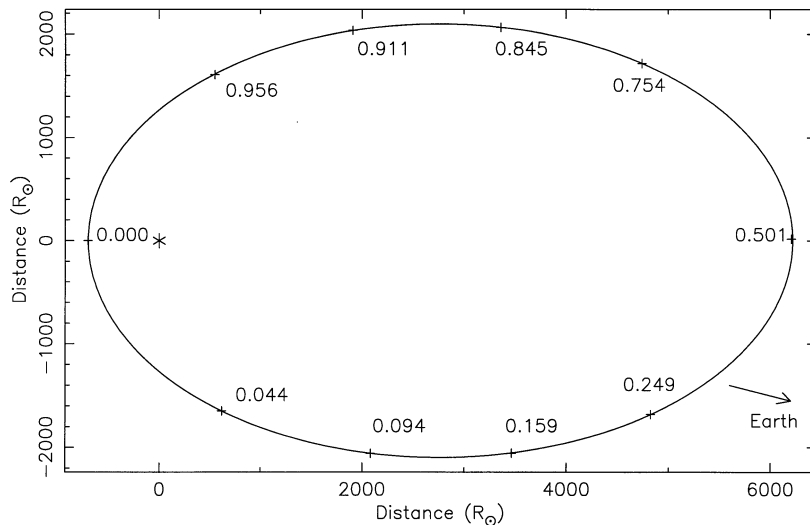


Figure 1. Proposed orbit for Eta Car in the frame of reference of the LBV primary (LBV at the origin, marked with an asterisk). The direction of Earth is marked with an arrow. At periastron the line of sight into the system is through the massive LBV wind. The phase is indicated at a number of positions.

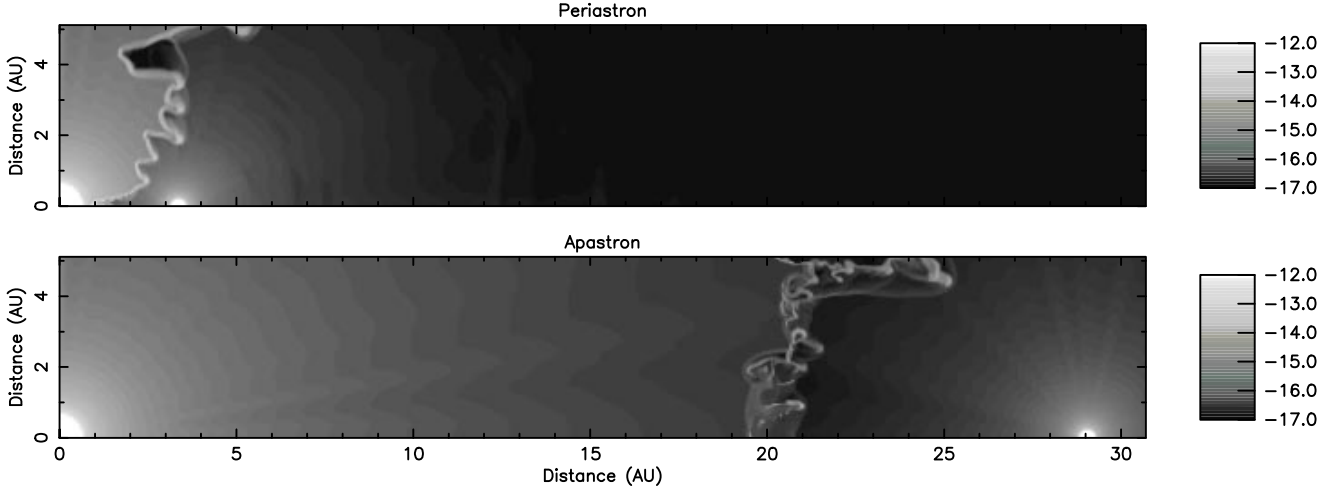


Figure 2. Log density plots (g cm^{-3}) of the numerical simulation. The top frame shows a ‘snapshot’ of the colliding wind at periastron, whilst the bottom frame is a ‘snapshot’ at apastron.

The frames were taken at periastron (top) and at apastron (bottom). The colliding-wind shock remains detached from both stars at all times throughout the orbit. Both shocked winds are strongly cooling at periastron, although the wind of the secondary becomes adiabatic at apastron. The post-shock flow is very unstable, and is believed to be a manifestation of the thin-shell instability (Stevens et al. 1992). Variable pre-shock velocities were obtained during the simulation as the secondary star penetrated deep into the acceleration zone of the primary wind at periastron. Along the line of centres the pre-shock velocities were 430–930 for the wind of the primary and 1380–1630 for the wind of the secondary. Neither sudden radiative braking nor radiative inhibition was seen, to any significant degree, in these simulations (Gayley, Owocki & Cranmer 1997; Stevens & Pollock 1994). This was expected, as *Eta Car* is a wide binary, and these effects are most significant when the stars are close. The self-consistent inclusion of radiative driving is required, however, because of the variable pre-shock velocities that are obtained.

The intrinsic (unabsorbed) X-ray emission calculated in our colliding-wind simulation scales inversely proportional to the separation distance of the two stars (see Pittard & Stevens 1997). Throughout most of the 5.52-yr orbit, the intrinsic emission is around $2.5 \times 10^{33} \text{ erg s}^{-1}$ for the 2.0–10.0 keV band. However, a sharp peak occurs at periastron, as the intrinsic emission in this band increases by an order of magnitude. There are two reasons for this: first, a greater fraction of the stellar winds are shocked; and secondly, the post-shock gas becomes increasingly radiative as the higher pre-shock densities and lower pre-shock velocities result in stronger cooling. The latter effect is expected to be the dominant one. Simulations of the eccentric long-period WR+O binary HD 193793 (Stevens et al. 1992) show a similar intrinsic X-ray light curve. Finally, we note that, on the finite-sized grid used, we estimate that we only capture ~ 50 per cent of the total emission, although the qualitative behaviour of the X-ray light curve is unaffected.

Fig. 3 shows the attenuated light curve in the 2.0–10.0 keV band after taking into account circumstellar and interstellar absorption. The luminosity is roughly constant with phase for much of the orbit, but begins to rise as periastron is approached because of the increase in the intrinsic emission. However, whereas the intrinsic emission peaks at approximately phase $\phi = 1.00$, the attenuated emission peaks at phase 0.94, and rapidly decreases thereafter. This is because although the intrinsic emission is increasing, the

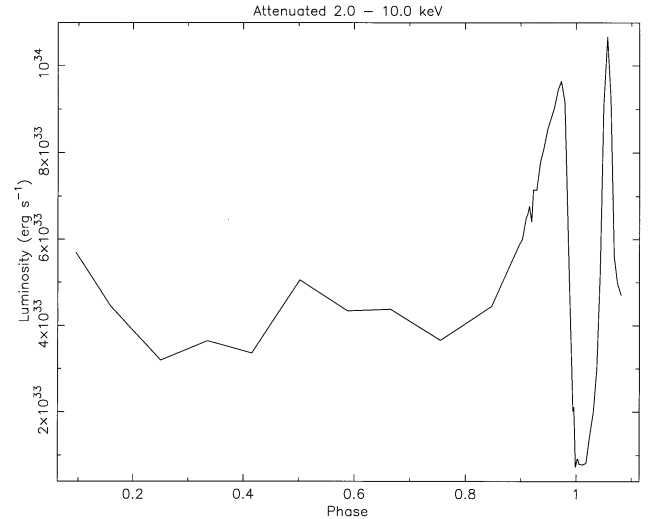


Figure 3. Attenuated 2.0–10.0 keV *RXTE* synthetic light curve generated from our hydrodynamic model.

attenuating column is also rapidly increasing as the line of sight begins to pass through the more massive LBV wind. Superimposed on top of this underlying trend is a significant amount of variability (which has been smoothed in Fig. 3). A Fourier analysis finds no excess power at the 85-d period seen in the *RXTE* light curve (Corcoran et al. 1997), supporting the view of Davidson, Ishibashi & Corcoran (1998) that this period represents either pulsation or rotation of the primary star (although a triple system cannot be ruled out; see Livio & Pringle 1998). The X-ray variability in our case is caused solely by the unstable nature of the colliding-wind shock in our simulation, and is reduced when we make our grid larger.

The 2.0–10.0 keV emission detected by the *ASCA* satellite during an observation at phase ~ 0.75 was $\sim 5.0 \times 10^{34} \text{ erg s}^{-1}$ (Corcoran et al. 1998b), which is approximately a factor of 6 times larger than in our simulation (if we assume that only 50 per cent of the total emission is captured by the grid). To account for this, the mass-loss rate of the primary probably needs to be increased.

Following the normal analysis technique of ‘real’ X-ray data, our synthetic X-ray spectra have been fitted with two-temperature Raymond–Smith models with separate absorbing columns. The results are shown in Fig. 4. There is a strong rise in absorbing

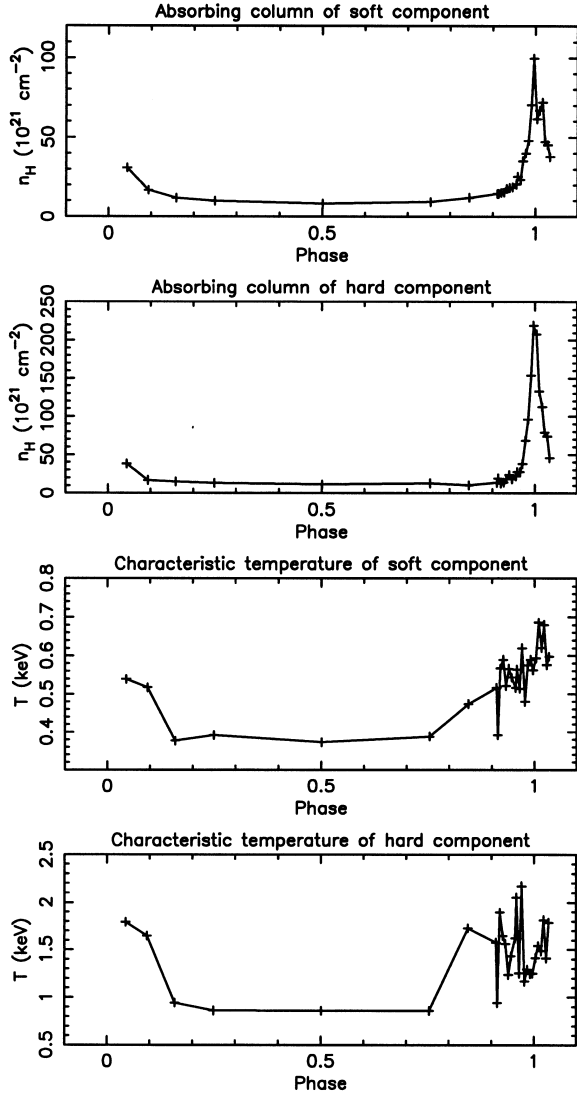


Figure 4. Spectral fit results to the synthetic spectra generated from our hydrodynamic model, as a function of orbital phase. We have concentrated on the periastron passage. Note the sharp peaks in the absorbing columns at this time.

column around periastron, responsible for the minimum in the light curve. The characteristic temperatures of both Raymond–Smith components also appear to increase around periastron, although it is not obvious why this is so. The terminal velocity of the secondary should also be increased in future models, in order for the high-temperature component to match more closely the characteristic temperature obtained from actual observations.

The rise in the 2.0–10.0 keV luminosity between phases 0.68 and 0.93 in the synthetic light curve is in qualitative agreement with the observed light curve. The minimum in the synthetic light curve has a duration of approximately 3–4 months. If our predictions are correct, the *RXTE* count rate should rise sharply to $\sim 60 \text{ count s}^{-1}$ and peak sometime around the end of 1998 March, before falling rapidly back to the quiescent level of $\sim 30 \text{ count s}^{-1}$. This is similar to the behaviour of the X-ray emission seen in the most recent *RXTE* observations (Corcoran et al. 1998b), where the start of ‘recovery’ was reported.

While there is good qualitative agreement between the temporal behaviour of the observed X-ray light curve and the synthetic

colliding-wind X-ray light curve, there are some discrepancies between the observed and model spectral variability. A preliminary analysis of an *ASCA* spectrum obtained on 1997 December 24 shows that the *intrinsic* luminosity of the source is *low* (and not high) at periastron, whilst the absorbing column is fairly low too (Corcoran et al., in preparation). This is in conflict with the simulations presented here, which predict the opposite. However, this discrepancy can be resolved if the extent of the hard X-ray emission is considerably larger than the volume explored in our model and an extra source of opacity which entirely absorbs the hard emission close to the stars is present. In such a scenario, the latter phenomenon accounts for the reduction in emission measure, whilst the former accounts for the remaining hard emission (at relatively low absorption) which originates outside the ‘occulted zone’. The current simulations do not cover a large enough volume to capture all of the X-ray emission, so this proposal is plausible. Detailed spectral modelling will be performed in a further paper.

4 DISCUSSION

We have demonstrated that the long-term X-ray variability seen in the *RXTE* PCA light curve is qualitatively similar to that expected from a colliding-wind model, providing further support for the binary model of Eta Car. In particular, the model predicts a rise in the observed X-ray emission towards periastron, followed by a sharp drop and subsequent recovery. This is indeed what is seen in the *RXTE* light curve. More models are needed, but colliding winds are able to provide a robust explanation of the observed X-ray light curve. We also note that Eta Car has several other features in common with HD 193793 (Williams et al. 1990), including a rapid decline of X-ray, radio and mm flux near periastron (Corcoran 1995; Corcoran et al. 1995; Duncan et al. 1995; Cox et al. 1995), peaks in the near-IR light curve around periastron (Whitelock et al. 1994) and almost constant fluxes and colour indices at optical and UV ranges. All are signatures of a colliding-wind system.

ACKNOWLEDGMENTS

The numerical simulations were computed at the Birmingham Starlink node. We thank the referee for helpful comments. JMP and IRS acknowledge funding from the School of Physics & Astronomy and PPARC respectively.

REFERENCES

- Castor J. I., Abbott D. C., Klein R. I., 1975, *ApJ*, 195, 157
- Colella P., Woodward P. R., 1984 *J. Comput. Phys.*, 54, 174
- Corcoran M. F., 1995, *Rev. Mex. Astron. Astrofis.*, 5, 54
- Corcoran M. F., Rawley G. L., Swank J. H., Petre R., 1995, *ApJ*, 445, L121
- Corcoran M. F., Ishibashi K., Swank J. H., Davidson K., Petre R., Schmitt J. H. M. M., 1997, *Nat*, 390, 587
- Corcoran M. F. et al., 1998a, *ApJ*, 494, 381
- Corcoran M. F., Swank J. H., Petre R., Ishibashi K., Davidson K., 1998b, *IAU Circ.* 6842
- Cox P., Mezger P. G., Sievers A., Najarro F., Bronfman L., Kreysa E., Haslam G., 1995, *A&A*, 297, 168
- Damineli A., 1996, *ApJ*, 460, L49
- Damineli A., Conti P. S., Lopes D. F., 1997, *New Astron.*, 2, 107
- Davidson K., 1989, in Davidson K., Moffat A. F. J., Lamers H., eds, *IAU Colloq.* 113, *Physics of Luminous Blue Variables*. Kluwer, Dordrecht p. 101
- Davidson K., 1997, *New Astron.*, 2, 387
- Davidson K., Humphreys R. M., 1997, *ARA&A*, 35, 1

- Davidson K., Walborn N. R., Gull T. R., 1982, ApJ, 254, L47
Davidson K., Ishibashi K., Corcoran M. F., 1998, New Astron., submitted
Duncan R. A., White S. M., Lim J., Nelson G. J., Drake S. A., Kundu M. R.,
1995, ApJ, 441, L73
Gayley K. G., Owocki S. P., Cranmer S. R., 1997, ApJ, 475, 786
Humphreys R., Davidson K., 1994, PASP, 106, 1025
Livio M., Pringle J. E., 1998, MNRAS, 295, L59
Pittard J. M., 1998, MNRAS, in press
Pittard J. M., Stevens I. R., 1997, MNRAS, 292, 298
Raymond J. C., Smith B. W., 1977, ApJS, 35, 419
Stevens I. R., Pollock A. M. T., 1994, MNRAS, 269, 226
Stevens I. R., Blondin J. M., Pollock A. M. T., 1992, ApJ, 386, 265
van Genderen A. M., de Groot M. J. H., Thé P. S., 1994, A&A, 283, 89
White S. M., Duncan R. A., Lim J., Nelson G. J., Drake S. A., Kundu M. R.,
1994, ApJ, 429, 380
Whitelock P. A., Feast M. W., Koen C., Roberts G., Carter B. S., 1994,
MNRAS, 270, 364
Williams P. M., van der Hucht K. A., Pollock A. M. T., Florkowski D. R.,
van der Woerd H., Wamsteker W. M., 1990, MNRAS, 243, 662
Willis A. J., Schild H., Stevens I. R., 1995, A&A, 298, 549

This paper has been typeset from a $\text{T}_{\text{E}}\text{X}/\text{L}^{\text{A}}\text{T}_{\text{E}}\text{X}$ file prepared by the author.